Effect of localized current distributions in periodically nanostructured OLEDs on the resonant light outcoupling

Lüder, Hannes, Buhl, Janek, Gerken, Martina

Hannes Lüder, Janek Buhl, Martina Gerken, "Effect of localized current distributions in periodically nanostructured OLEDs on the resonant light outcoupling," Proc. SPIE 11995, Physics and Simulation of Optoelectronic Devices XXX, 119950A (4 March 2022); doi: 10.1117/12.2606225

SPIE.

Event: SPIE OPTO, 2022, San Francisco, California, United States

Effect of localized current distributions in periodically nanostructured OLEDs on the resonant light outcoupling

Hannes Lüder, Janek Buhl, and Martina Gerken

Chair for Integrated Systems and Photonics, Faculty of Engineering, Kiel University

ABSTRACT

We present an electrical and optical model for simulating the current distribution in and the resonant light emission from nanostructured organic light-emitting diodes (OLEDs). A periodic nanostructure in an OLED can be used as a resonant waveguide grating to tailor the light emission, i.e., to direct the dominant emission wavelength into a specific direction. We show that the current injection at nanostructured electrodes is strongly enhanced at their corners, leading to localized current paths and emission zones. These current paths have to be overlapping with the resonant optical field hot spots in order to gain maximal resonant light outcoupling. We show that this is not generally the case for periodically nanostructured OLEDs and that the introduction of local isolation layers can improve the overlap by altering the current paths. Depending on the isolation layer configuration either the resonant or non-resonant light outcoupling is pronounced. This optimization potential may be beneficial for compact organic optoelectronic sensors that require highly directional OLED emission.

Keywords: Organic light-emitting diode, nanostructure, charge carrier distribution, finite element method, localized emission, resonant waveguide grating, photonic crystal slab, resonant light outcoupling

1. INTRODUCTION

Organic light-emitting diodes (OLEDs) are versatile light sources with application areas ranging from general lighting,[1] automotive applications,[2] and displays[3] to specialized integrated lab-on-chip sensors.[4] One promising key feature of OLEDs is the potential mass-manufacturability using roll-to-roll print technologies, which would enable cost-efficient high-volume fabrication. This makes printed organic optoelectronics especially interesting for inexpensive integrated single-use point-of-care lab-on-chip sensors. Current research on integrated organic optoelectronic sensors often uses side-by-side configurations of OLEDs and OPDs (organic photodetectors), for example in pulse oximetry[5–7] or fluorescence sensing.[8] In such OLED OPD configurations, directional light emission from the OLED may be beneficial in order to maximize the amount of light that reaches the sensing area that is covered by the OPD (see Fig. 1 (a)).

However, OLEDs are large-area surface emitters with approximately Lambertian emission profiles.[9] Due to their thin-film structure, the organic layers form an optical waveguide which traps part of the created photons in guided modes.[10] Especially these waveguide modes can be utilized to achieve directional light outcoupling by integrating a periodic nanostructure with a period at the scale of the wavelength of light into the OLED stack. This creates optical resonances which direct the dominant emission wavelength into a specific direction.[11] These optical resonances with localized field enhancements have the additional effect that the spectra and emission patterns of the emitting molecules are strongly influenced by their individual positions with respect to the nanostructure.[12,13]

Such light-extraction technique that directly accesses the guided optical modes in the organic layers will change the geometry of the OLED stack and thereby also influence the OLED's electric behavior.[14,15] Sharp corners concentrate the charge injection at their positions due to the local field enhancement[16,17] (see Fig. 1 (c) for an example) and local changes in minimum electrode distance modify the location of the dominant current paths through such a nanostructured device and thereby the location and shape of the main emission zones,

Further author information: (Send correspondence to M.G.)
H.L.: E-mail: halu@tf.uni-kiel.de, J.B.: E-mail: jabu@tf.uni-kiel.de, M.G.: E-mail: mge@tf.uni-kiel.de
Telephone: +49 431 880 6250, Postal address: Technische Fakultät, Kaiserstr. 2, 24143 Kiel, GERMANY

Physics and Simulation of Optoelectronic Devices XXX, edited by Bernd Witzigmann, Marek Osiński, Yasuhiko Arakawa, Proc. of SPIE Vol. 11995, 119950A
 · 0277-786X · doi: 10.1117/12.2606225

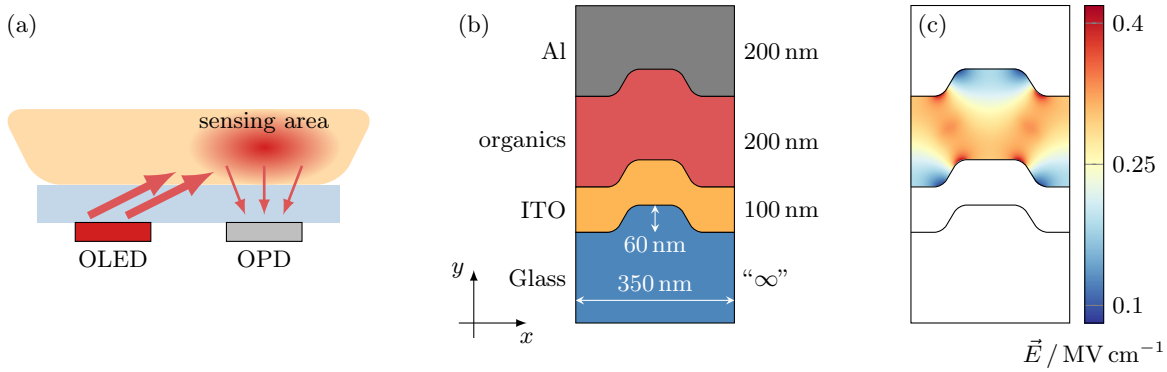

Figure 1. (a) Application example for directional OLED emission: OLED and OPD are manufactured side by side on one substrate. The OLED illuminates the sensing area (e.g. the human skin for pulse oximetry or a fluorescent layer for a fluorescence-based sensor) above the OPD. Directional emission maximizes the light utilization. (b) Schematic of the structure under investigation. One unit cell of the periodically nanostructured simplified OLED is shown. We assume a 1D grating with period 350 nm and 60 nm ridge height on a glass substrate with 60° edge angles and 30 nm corner radii (In an actual device, the grating could be fabricated, e.g. into a nanoimprint resist layer on top of the glass substrate.[18]) and subsequently deposited transparent anode (indium tin oxide, ITO), organic layers, and metallic cathode (aluminum, Al), that adopt the substrate grating's shape. The electric model's domain is only the organics layer, while the optical model includes the complete stack. (c) Example result for the electric field enhancement at the electrode corners when a voltage of 5 V is applied. (A planar 200 nm thick device would have an average electric field of 0.25 MV cm^{-1}.) These field enhancements cause increased current injection, leading to localized current paths.

which, finally, influence the strength of resonant versus non-resonant light emission. Thus, optical and electrical design and optimization of nanostructures is interlinked.

In this work, we investigate theoretically how the localization of the current distribution in a periodically nanostructured OLED influences its emission spectrum and radiation pattern using the finite element method (FEM) and the finite-difference time-domain method (FDTD). In contrast to Fujita et al.,[14,15] we include charge transport properties of the organics layer into the electrical model in order to calculate charge carrier distributions and recombination zones in the nanostructured OLED. Our work focuses specifically on the local overlap between the recombination zones and the optical resonances in simplified nanostructured OLED models, and we investigate for the first time the alignment of optical and electrical effects by addition of electrical isolation areas in the OLED for current steering.

Figure 1 (b) shows a schematic of the simulated geometry. It represents a simplified bottom-emitting OLED with an ITO-organics-Al stack on a nanostructured glass substrate. As our aim is to investigate the principal effect, this simplification omits details such as the specific organic layer stack.

2. MODELING

In order to investigate the combined electrical and optical effects, we implemented models for both the electronic behavior and the electromagnetic fields at optical frequencies. We neglect coupling between the stationary currents and the optical fields. Therefore, the simulations can run sequentially and the location of the emission zones obtained from the electrical simulation is used to calculate the optical farfield from the electromagnetic simulation.

We implemented our electrical model in a weak-form FEM formulation using COMSOL Multiphysics.[19] For the optical simulations we used Lumerical's FDTD electromagnetic solver.[20] The main advantage of using COMSOL Multiphysics is the ability to solve all involved physics for exactly the same geometry on the identical mesh, but as the time-domain method is faster in this specific situation,[21] it is used for the optical simulations.

The investigated simplified devices are periodically structured in one dimension. The layers are stacked in the second dimension. The whole structure is invariant in the third dimension. Therefore, all simulations are restricted to a 2D unit cell.

2.1 The electrical model

The electrical behavior of the simplified OLED is described by the electric field $\vec{E}$, the electric potential ϕ, the hole and electron current densities $\vec{J}_\mathrm{h}$ and $\vec{J}_\mathrm{e}$, the hole and electron densities n_h and n_e, and the recombination rate r. The organic material has the properties permittivity $\varepsilon = \varepsilon_0\varepsilon_\mathrm{r}$, charge carrier mobility μ, and diffusion constant D. The governing equations for the aforementioned quantities are Gauß' law and continuity equations for both types of charge carriers:[22,23]

$$\operatorname{div}\vec{E} = q(n_\mathrm{h} - n_\mathrm{e}), \qquad \operatorname{div}\vec{J}_\mathrm{h} = -qr, \qquad \operatorname{div}\vec{J}_\mathrm{e} = qr, \tag{1}$$

where $q \approx 1.6 \times 10^{-19}\,\mathrm{A\,s}$ is the elementary charge, $\vec{E} = -\operatorname{grad}\phi$, and the currents include drift and diffusion currents:

$$\vec{J}_\mathrm{h} = qn_\mathrm{h}\mu\vec{E} - qD\operatorname{grad}n_\mathrm{h}, \qquad \vec{J}_\mathrm{e} = qn_\mathrm{e}\mu\vec{E} + qD\operatorname{grad}n_\mathrm{e}. \tag{2}$$

From the calculated charge carrier distributions, the recombination zones can be calculated assuming a Langevin-type recombination:[23] $r = \gamma n_\mathrm{h} n_\mathrm{e}$.

COMSOL does not include a module tailored to organic semiconductors, where the current is driven by injected, not intrinsic, charges. Therefore, we implemented the above equations in the "Weak Form PDE" interface using fourth-order Lagrange elements for the electric potential ϕ and second-order Lagrange elements for the charge carrier densities n_h and n_e.[24]

The organic material's mobility is described by the Poole-Frenkel dependence[23] $\mu(E) = \mu_0 \exp(\beta\sqrt{E})$ and the diffusion constant by the Einstein relation[25] $D = \frac{k_\mathrm{B}T}{q}\mu$ (k_B: Boltzmann constant, T: temperature). The boundary conditions are set as follows: For all non-electrode boundaries, $\vec{n}\cdot\varepsilon\vec{E} = 0$ and $\vec{n}\cdot\vec{J}_{\{\mathrm{h,e}\}} = 0$ (Neumann boundary conditions), where $\vec{n}$ is an outward unit normal vector on the boundary. The electrode boundaries are described by specifying ϕ (Dirichlet boundary condition) and the (field-dependent) injected current $\vec{J}_{\mathrm{inj,\,e}}$ or $\vec{J}_{\mathrm{inj,\,h}}$, respectively. The condition on the opposing boundary for the respective carrier type has barely any influence on the simulation results and can be set to either $n_\mathrm{h} = 0$, $n_\mathrm{e} = 0$ or $\vec{n}\cdot\operatorname{grad}n_\mathrm{h} = 0$, $\vec{n}\cdot\operatorname{grad}n_\mathrm{e} = 0$. The results presented here are calculated with the second type of boundary conditions.

The charge injection at the metal-organic interfaces can be described by various models, among which Richardson-Schottky thermionic emission and Fowler-Nordheim tunneling are the simplest.[22] We use the injection model by Emtage and O'Dwyer,[26] which is based on thermionic emission and agrees well with Wolf et al.'s model of injection into a disordered hopping system,[27] but has a much simpler analytic description. We combine Emtage and O'Dwyer's low- and high-field approximations into the single expression

$$J_\mathrm{inj} = \big(1 - \mathrm{sigmoid}(f)\big)\left(\alpha^* f\right) + \mathrm{sigmoid}(f)\left(\alpha^*\left(\frac{4}{\pi^2}f^3\right)^{1/4}\exp\left(\sqrt{f}\right)\right), \qquad f = \beta^{*2}E \tag{3}$$

with the sigmoid function $\mathrm{sigmoid}(f) = f^2/(1+f^2)$, which realizes the smooth transition from the low- to the high-field approximation. The parameter values used in the electrical simulations are summarized in Table 1.

The major simplification in this model is that the organic stack is modeled by just one homogeneous layer with the same charge transport and injection properties for holes and electrons, i.e. the HOMO and LUMO levels of the different layers found in an actual OLED and the interface effects between those layers are not taken into account. Although this is quite a simplification, it is justified as long as only the principal effects of the nanostructure on the current paths and emission zone positions and the resulting principal implications on the optical far fields are considered. The symmetric injection and transport properties for holes and electrons ensure a balance of charge carriers that would be achieved in an actual OLED by properly designed transport and blocking layers.

Table 1. Material parameters used in the simulations. The mobility parameters are taken from Brütting et al.[22] for the exemplary organic material NPB material. The injection parameters are estimated from fabricated and characterized hole-only devices, also with NPB. The refractive index dispersion for aluminum is taken from McPeak et al.[28,29] For the other optical materials, representative values have been chosen instead of detailed dispersion curves.

electrical		optical	
ε_r	3.0	n_Al	(McPeak)
μ_0	$1 \times 10^{-8}\,\mathrm{m^2/V/s}$	n_organics	$1.8 + 0.01\mathrm{i}$
β	$150 \times 10^{-6}\,\sqrt{\mathrm{m/V}}$	n_ITO	$1.9 + 0.005\mathrm{i}$
α^*	$500\,\mu\mathrm{A/m^2}$	n_glass	1.52
β^*	$2 \times 10^{-3}\,\sqrt{\mathrm{m/V}}$		
γ	$1 \times 10^{-14}\,\mathrm{m^3/s}$		
T	294.15 K		

2.2 The optical model

After the recombination zones, i.e. the emission zones, have been calculated with the electrical model, the optical simulation calculates the emitted light from emitters continuously distributed in the emission zones according to r. As the introduction of a light-emitting dipole into the model breaks the periodicity of the simulated system, the simulation of a long (up to several hundred periods) section of the periodically nanostructured waveguide would be necessary.[12] As a more efficient approach, we use a reciprocity-based approach,[30,31] which exchanges the role of the source dipole in the OLED stack and the observation point in the far field to excitation with a source dipole in the far field and observation at the former source position in the OLED stack. The far away dipole source essentially creates plane waves incident to the OLED stack. Without the dipole in the stack, the periodicity is restored. Furthermore, the effect of all emitters in the emission zones can be calculated from one single simulation. To obtain the full angular resolved far field, this simulation has to be performed for all angles and wavelengths of interest.

We use Lumerical FDTD to solve the source-free Maxwell's equations[32]

$$\begin{aligned} \operatorname{curl} \mu^{-1} \vec{B} &= \varepsilon \frac{\partial \vec{E}}{\partial t}, \\ \operatorname{curl} \vec{E} &= -\frac{\partial \vec{B}}{\partial t}, \\ \operatorname{div} \varepsilon \vec{E} &= 0, \\ \operatorname{div} \vec{B} &= 0, \end{aligned} \tag{4}$$

where $\vec{E}$ and $\vec{B}$ are the electric and magnetic field and ε and μ are the permittivity and permability (not to be confused with the mobility μ in the electrical model).

The FDTD simulation is set up as follows: The left and right boundaries have Floquet boundary conditions and the top and bottom boundaries are set to PEC (perfect electric conductor). To mimic the free space, a PML (perfectly matched layer) is used at the bottom boundary (12 layers, profile type "steep angle") after 1000 nm substrate. The incident wave is excited using a BFAST plane wave source.[33] The refractive indices $n = \sqrt{\varepsilon_\mathrm{r}}$ used in the simulation can be found in Table 1.

After the electromagnetic field excited by the incident plane wave has been calculated, the far-field radiation intensity pattern $I(\lambda, \vartheta)$ is obtained by means of the reciprocity principle by integrating the contributions of all recombination zones:[30,31]

$$I(\lambda, \vartheta) \propto \frac{1}{\lambda^4} \iint\limits_\mathrm{organics} r \left| \underline{\vec{E}}(\lambda, \vartheta) \cdot \vec{p} \right|^2 \mathrm{d}A, \tag{5}$$

where λ is the vacuum wavelength, r the recombination rate from the electrical simulation, $\underline{\vec{E}}(\lambda, \vartheta)$ the electric field phasor in the OLED stack excited by the wave with incidence angle ϑ, and $\vec{p}$ the assumed dipole orientation

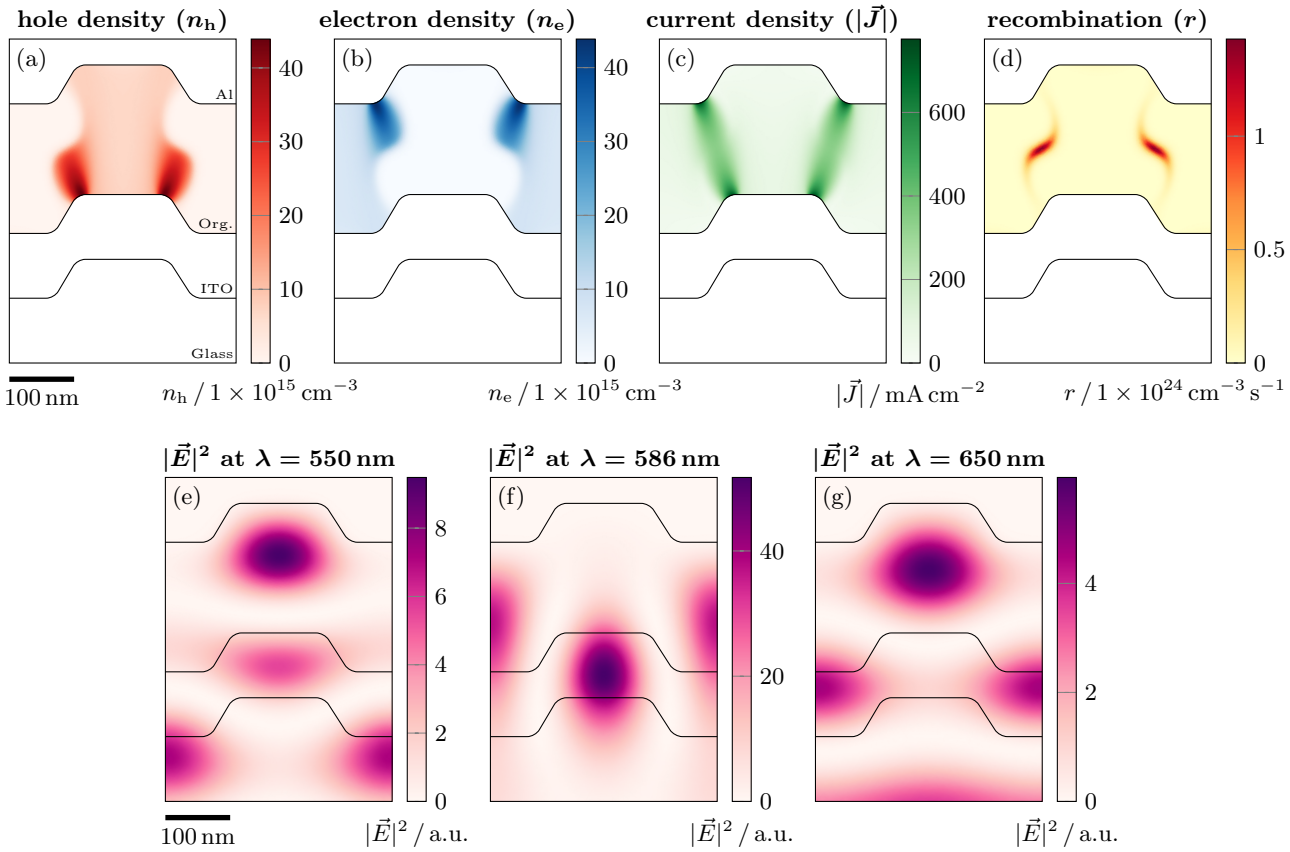

Figure 2. Field distributions inside the analyzed device. (a) Hole density. (b) Electron density. (d) Current density. (d) Recombination rate. (e)–(g) Optical field below, at, and above resonance (TE polarization, $\vec{E} = E_z\vec{e}_z$). It can be seen that the recombination areas are neither well aligned with areas of resonantly enhanced optical intensities nor with the off-resonant field distributions.

for the light-emitting molecule. This work focuses on TE polarized light, which is the dominant polarization emitted from spin-coated conjugated polymer emission layers.[34] Therefore, $\vec{E} = E_z\vec{e}_z$ throughout the analysis. Note that all proportionality factors have been omitted from the above expression because they are of no importance in this study.

The interplay of electrical and optical effects makes a fair comparison of different devices difficult. Increased currents, e.g., due to enhanced current injection lead to higher values of r and consequently to an increased radiation intensity. To separate such influences from the main investigation focus, the spatial overlap between recombination zones and optical resonances, we used the normalized recombination $r_{\mathrm{norm}} = r/\iint r\,\mathrm{d}A$ instead of r in Eq. (5). Thereby, all optical far fields can be thought of as created from the same number of photons.

3. RESULTS

Figure 2 shows the charge carrier densities, current densities, recombination zones and the optical field intensity at resonant and non-resonant wavelengths. At resonance, the largest optical field inside the organic layer is in the grating groove, whereas off resonance the largest field is found above the grating ridge. In contrast, the current mainly flows between adjacent grating edges, where also the main recombination zones are located. Therefore, we expect suboptimal resonance effects for this structure. The optimum resonant light outcoupling is expected when the recombination zones are aligned with the optical fields at resonance. We tested the idea of isolating parts of the electrode with a thin (10 nm) isolation layer in order to force the current to the grating ridge or grating groove regions. Figure 3 shows the charge carrier densities, current flows and recombination zones for structures

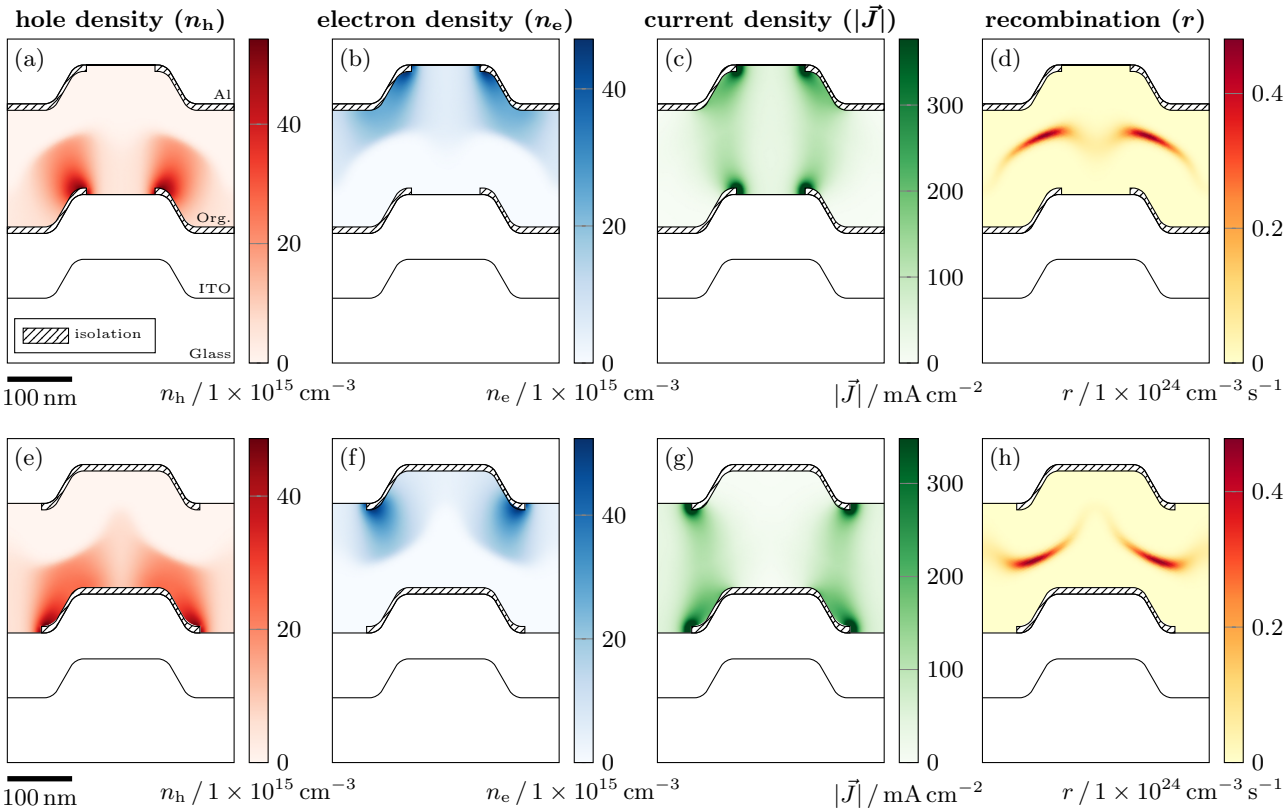

Figure 3. Field distributions inside device with partly isolated electrodes. Top row: current injection only from the grating ridges, bottom row: current injection only from the grating grooves. The hatched areas indicate the isolation layers. (a), (e) Hole density. (b), (f) Electron density. (c), (g) Current density. (d), (h) Recombination rate. Compared to Fig. 2 (d), the recombination areas extend further horizontally. The recombination areas in (d) seem better aligned with the off-resonant optical fields in Fig. 2, while in (h) it seems better aligned with the optical field at resonance.

with isolated grating edges and either isolated grating ridges or grooves. Interestingly, the charge carriers diffuse significantly into the regions left and right of the expected direct current paths.

The spectral intensities of the outcoupled light are shown in Fig. 4 and Fig. 5. It can be seen that isolating the grating ridge results in the highest resonant light outcoupling and also the strongest suppression of non-resonant background light. In contrast, isolating the grating groove enhances the non-resonant and reduces resonant light. This is in accordance with the results from Fig. 3 and Fig. 2 (e)–(f): The current density and recombination in the ridge-isolated device align better with the resonant optical field, whereas they align better with the non-resonant optical fields in the groove-isolated device.

4. SUMMARY AND OUTLOOK

We developed and implemented a simplified electrical model for nanostructured OLEDs using the finite element method. Combined with an optical solver, this allows to investigate the combined electrical and optical effects of integrated nanostructures in organic optoelectronic devices. As an example, we showed that the current paths and recombination zones in a device with a simple periodic grating as the nanostructure do not well align with the optical resonances. With the addition of thin isolation layers that partly cover the electrode, a better alignment is possible. In this work, however, the isolation layers suppress the enhanced current injection at the grating corners, thereby possibly reducing the overall efficiency. Best results can be expected from optimized nanostructures that bring together the enhancements from increased current injection and the optical resonances.

One point not discussed in this paper is surface roughness, which creates additional charge injection hot spots all over the electrodes, possibly leading to a broader current distribution in the device. However, first

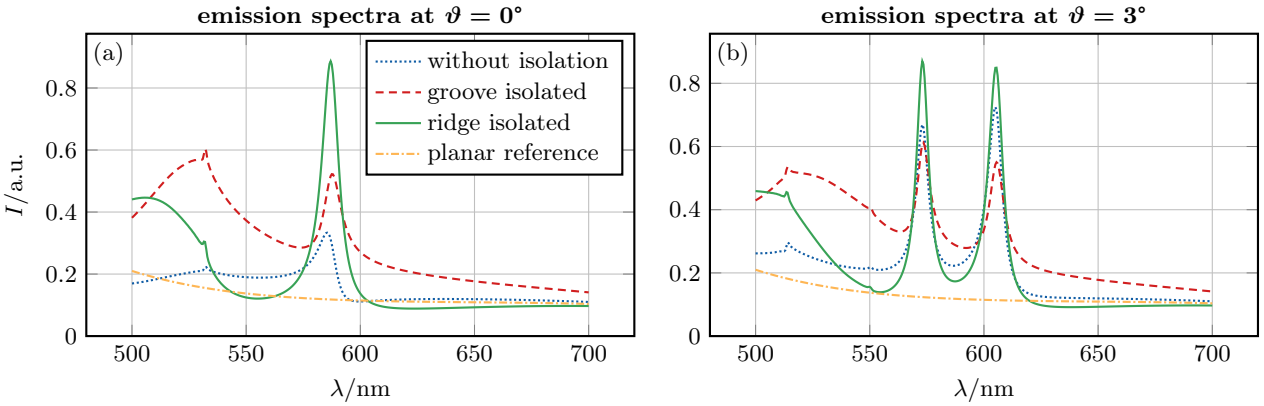

Figure 4. Emission spectra for the different analyzed devices for perpendicular emission ($\vartheta = 0°$, (a)) and emission at $\vartheta = 3°$ (b). The device with isolated grating grooves (green, solid lines) shows the strongest optical resonance and also the largest peak-to-background ratio, while this is reversed for the device with isolated grating ridges (red, dashed lines), which has a large non-resonant and only weakly enhanced emission. The planar reference curve (orange, dash-dotted lines) shows the emission spectrum from a non-structured planar device. Note that band gap effects inhibit the excitation of the resonance in the device without isolation layers (blue, dotted lines) exactly at $\vartheta = 0°$. Therefore, (b) shows the emission spectra for $\vartheta = 3°$ in order to present a more representative case. The band gap effect can also be seen in Fig. 5 (a).

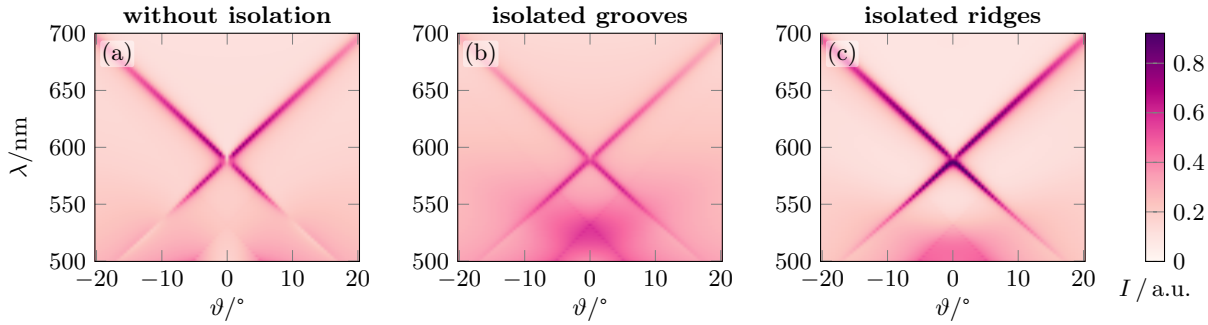

Figure 5. Angle-resolved emission spectra (far fields) for the non-isolated (a), the groove-isolated (b), and the ridge-isolated (c) device. The characteristic resonance cross is prominent in all cases. However, compared to the non-isolated case, it is weakened for the groove-isolated and enhanced for the ridge-isolated device. Correspondingly, the groove-isolated device has the highest non-resonant emission, while the ridge-isolated has the lowest. This observation is in accordance with the recombination zone locations in Fig. 3.

simulations show that the dominant emission zones and the resulting optical far fields remain rather unchanged. Experimental investigations could reveal whether the simulated changes of the angular emissions spectra are observable in actual OLEDs. The fabrication of the necessary local isolation layers may be achieved using oblique deposition techniques[35,36] or lithography based on anisotropic etching.[37]

We believe that the combined electrical and optical optimization of nanostructured OLEDs, taking into account the localized fields, can considerably improve the resonance-to-background ratio of the directionally outcoupled light, which is especially important for the development of compact integrated photonic lab-on-chip sensors.

ACKNOWLEDGMENTS

The authors acknowledge support by Interreg (Project Rollflex, 1_11.12.2014). This project has received funding partly from the European Research Council (ERC) under the European Union's Horizon 2020 research and innovation programme (BEAMOLED, grant agreement No. 899861).

REFERENCES

[1] Phelan, G. M., "OLED Lighting Hits the Market," *Information Display* **34**(1), 10–15 (2018).

[2] Chowdhury, D. Q., Garner, S. M., and Lewis, S. C., "Application of OLED for Automotive Lighting," in [*2019 26th International Workshop on Active-Matrix Flatpanel Displays and Devices (AM-FPD)*], **26th**, 1–3 (July 2019).

[3] Huang, Y., Hsiang, E.-L., Deng, M.-Y., and Wu, S.-T., "Mini-LED, Micro-LED and OLED displays: present status and future perspectives," *Light: Science & Applications* **9**, 105 (June 2020).

[4] Venkatraman, V. and Steckl, A. J., "Quantitative Detection in Lateral Flow Immunoassay Using Integrated Organic Optoelectronics," *IEEE Sensors Journal* **17**, 8343–8349 (Dec. 2017).

[5] Lee, H., Kim, E., Lee, Y., Kim, H., Lee, J., Kim, M., Yoo, H.-J., and Yoo, S., "Toward all-day wearable health monitoring: An ultralow-power, reflective organic pulse oximetry sensing patch," *Science Advances* (Nov. 2018).

[6] Khan, Y., Han, D., Pierre, A., Ting, J., Wang, X., Lochner, C. M., Bovo, G., Yaacobi-Gross, N., Newsome, C., Wilson, R., and Arias, A. C., "A flexible organic reflectance oximeter array," *Proceedings of the National Academy of Sciences* **115**, E11015–E11024 (Nov. 2018).

[7] Elsamnah, F., Bilgaiyan, A., Affiq, M., Shim, C.-H., Ishidai, H., and Hattori, R., "Reflectance-Based Organic Pulse Meter Sensor for Wireless Monitoring of Photoplethysmogram Signal," *Biosensors* **9**, 87 (Sept. 2019).

[8] Titov, I., Köpke, M., Schneidewind, N. C., Buhl, J., Murat, Y., and Gerken, M., "OLED-OPD Matrix for Sensing on a Single Flexible Substrate," *IEEE Sensors Journal* **20**, 7540–7547 (July 2020).

[9] Kim, J.-S., Ho, P. K. H., Greenham, N. C., and Friend, R. H., "Electroluminescence emission pattern of organic light-emitting diodes: Implications for device efficiency calculations," *Journal of Applied Physics* **88**, 1073–1081 (July 2000).

[10] Meerheim, R., Furno, M., Hofmann, S., Lüssem, B., and Leo, K., "Quantification of energy loss mechanisms in organic light-emitting diodes," *Applied Physics Letters* **97**, 253305 (Dec. 2010).

[11] Geyer, U., Hauss, J., Riedel, B., Gleiss, S., Lemmer, U., and Gerken, M., "Large-scale patterning of indium tin oxide electrodes for guided mode extraction from organic light-emitting diodes," *Journal of Applied Physics* **104**, 093111 (Nov. 2008).

[12] Lüder, H. and Gerken, M., "FDTD modelling of nanostructured OLEDs: analysis of simulation parameters for accurate radiation patterns," *Optical and Quantum Electronics* **51**, 139 (Apr. 2019).

[13] Li, Y., Kovačič, M., Westphalen, J., Oswald, S., Ma, Z., Hänisch, C., Will, P.-A., Jiang, L., Junghaehnel, M., Scholz, R., Lenk, S., and Reineke, S., "Tailor-made nanostructures bridging chaos and order for highly efficient white organic light-emitting diodes," *Nature Communications* **10**, 2972 (July 2019).

[14] Fujita, M., Ueno, T., Ishihara, K., Asano, T., Noda, S., Ohata, H., Tsuji, T., Nakada, H., and Shimoji, N., "Reduction of operating voltage in organic light-emitting diode by corrugated photonic crystal structure," *Applied Physics Letters* **85**, 5769–5771 (Dec. 2004).

[15] Fujita, M., Ishihara, K., Ueno, T., Asano, T., Noda, S., Ohata, H., Tsuji, T., Nakada, H., and Shimoji, N., "Optical and Electrical Characteristics of Organic Light-Emitting Diodes with Two-Dimensional Photonic Crystals in Organic/Electrode Layers," *Japanese Journal of Applied Physics* **44**, 3669 (June 2005).

[16] Bian, Q., Musumeci, C., Wang, C., Skallberg, A., Chen, Y., Hu, Z., Peter Münger, E., Uvdal, K., Fahlman, M., and Inganäs, O., "Nanocontacts give efficient hole injection in organic electronics," *Science Bulletin* **66**, 875–879 (May 2021).

[17] Choi, H.-H., Kim, M., Jang, J., Lee, K. H., Jho, J. Y., and Park, J. H., "Tip-enhanced electric field-driven efficient charge injection and transport in organic material-based resistive memories," *Applied Materials Today* **20**, 100746 (Sept. 2020).

[18] Jahns, S., Bräu, M., Meyer, B.-O., Karrock, T., Gutekunst, S. B., Blohm, L., Selhuber-Unkel, C., Buhmann, R., Nazirizadeh, Y., and Gerken, M., "Handheld imaging photonic crystal biosensor for multiplexed, label-free protein detection," *Biomedical Optics Express* **6**, 3724–3736 (Oct. 2015).

[19] "COMSOL Multiphysics." COMSOL Inc. (2021).

[20] "Lumerical FDTD." Lumerical Inc. (2021).

[21] Paulsen, M., Neustock, L. T., Jahns, S., Adam, J., and Gerken, M., "Simulation methods for multiperiodic and aperiodic nanostructured dielectric waveguides," *Optical and Quantum Electronics* **49**, 107 (Feb. 2017).

[22] Brütting, W., Berleb, S., and Mückl, A. G., "Device physics of organic light-emitting diodes based on molecular materials," *Organic Electronics* **2**, 1–36 (Mar. 2001).
[23] Köhler, A. and Bässler, H., [*Electronic processes in organic semiconductors: an introduction*], Wiley-VCH, Weinheim (2015).
[24] Brenner, S. and Scott, R., [*The Mathematical Theory of Finite Element Methods*], Texts in Applied Mathematics, Springer-Verlag, New York, third ed. (2008).
[25] Wetzelaer, G. A. H., Koster, L. J. A., and Blom, P. W. M., "Validity of the Einstein Relation in Disordered Organic Semiconductors," *Physical Review Letters* **107**, 066605 (Aug. 2011).
[26] Emtage, P. R. and O'Dwyer, J. J., "Richardson-Schottky Effect in Insulators," *Physical Review Letters* **16**, 356–358 (Feb. 1966).
[27] Wolf, U., Arkhipov, V. I., and Bässler, H., "Current injection from a metal to a disordered hopping system. I. Monte Carlo simulation," *Physical Review B* **59**, 7507–7513 (Mar. 1999).
[28] McPeak, K. M., Jayanti, S. V., Kress, S. J. P., Meyer, S., Iotti, S., Rossinelli, A., and Norris, D. J., "Plasmonic Films Can Easily Be Better: Rules and Recipes," *ACS Photonics* **2**, 326–333 (Mar. 2015).
[29] RefractiveIndex.INFO, "Refractive index of Al (Aluminium) – McPeak." https://refractiveindex.info/?shelf=main&book=Al&page=McPeak.
[30] Janssen, O. T. A., Wachters, A. J. H., and Urbach, H. P., "Efficient optimization method for the light extraction from periodically modulated LEDs using reciprocity," *Optics Express* **18**, 24522–24535 (Nov. 2010).
[31] Zhang, S., Martins, E. R., Diyaf, A. G., Wilson, J. I. B., Turnbull, G. A., and Samuel, I. D. W., "Calculation of the emission power distribution of microstructured OLEDs using the reciprocity theorem," *Synthetic Metals* **205**, 127–133 (July 2015).
[32] Jackson, J. D., [*Classical Electrodynamics*], John Wiley & Sons, Hoboken, New Jersey, third ed. (1999).
[33] "Lumerical BFAST Delivers Broadband Arbitrary Angle Capabilities for Periodic Devices – Lumerical." https://www.lumerical.com/learn/whitepapers/lumerical-bfast-delivers-broadband-arbitrary-angle-capabilities-for-periodic-devices/.
[34] Becker, H., Burns, S. E., and Friend, R. H., "Effect of metal films on the photoluminescence and electroluminescence of conjugated polymers," *Physical Review B* **56**, 1893–1905 (July 1997).
[35] Stroisch, M., Teiwes-Morin, C., Woggon, T., Gerken, M., Lemmer, U., Forberich, K., and Gombert, A., "Photonic stopband tuning of organic semiconductor distributed feedback lasers by oblique angle deposition of an intermediate high index layer," *Applied Physics Letters* **95**, 021112 (July 2009).
[36] Nazirizadeh, Y., von Oertzen, F., Karrock, T., Greve, J., and Gerken, M., "Enhanced sensitivity of photonic crystal slab transducers by oblique-angle layer deposition," *Optics Express* **21**, 18661–18670 (Aug. 2013).
[37] Buhl, J., Yoo, D., Köpke, M., and Gerken, M., "Two-Dimensional Nanograting Fabrication by Multistep Nanoimprint Lithography and Ion Beam Etching," *Nanomanufacturing* **1**, 39–48 (June 2021).